Journal of Environmental Management 395 (2025) 127916

Contents lists available at ScienceDirect

Journal of Environmental Management

journal homepage: www.elsevier.com/locate/jenvman

Research article

The role of climate in shaping vegetation dynamics and carbon dioxide fluxes in global protected forest landscapes

Md Rezaul Karim [a,*], Elham Ashrafizadeh [a], Md Shamim Reza Saimun [b], Wenxi Liao [c], Parvez Rana [d], Mohammed A.S. Arfin-Khan [b]

[a] Institute of Forestry and Conservation, John H. Daniels Faculty of Architecture, Landscape, and Design, University of Toronto, 33 Willcocks Street, Toronto, ON, M5S 3B3, Canada
[b] Department of Forestry and Environmental Science, School of Agriculture and Mineral Sciences, Shahjalal University of Science and Technology, Sylhet, 3114, Bangladesh
[c] Department of Chemical Engineering, McGill University, 3610 Rue University, Montreal, QC, H3A 0C5, Canada
[d] Natural Resources Institute Finland (Luke), Latokartanonkaari 9, FI-00790, Helsinki, Finland

ARTICLE INFO

Keywords:
Protected areas
Climate change
Carbon flux
Tree cover loss
Vegetation dynamics
Ecosystem resilience

ABSTRACT

Protected forest areas (PAs) are vital for biodiversity conservation, climate regulation, and carbon sequestration. Yet their ecological resilience faces increasing threats from climate change and human disturbances. Despite international efforts to expand PA coverage, the effectiveness of existing PAs in maintaining ecological functions under climate stress remains uncertain. To address this, we analyzed climate-driven vegetation dynamics, tree cover loss, and carbon dioxide (CO_2) fluxes across eight globally distributed tropical and temperate PAs between 2001 and 2023. Using climate datasets, MODIS-derived Gross Primary Productivity (GPP), vegetation indices (NDVI and EVI), tree cover loss products, and spatial carbon flux estimates, we assessed site-specific ecosystem responses to climate variability and forest degradation. Significant warming trends occurred at four sites (Crater Mountain, Białowieża, Tasmania, and Wolong), but significant precipitation changes were limited, decreasing in Crater Mountain and increasing in Wolong. GPP showed nonlinear temperature responses, peaking at 22–27 °C and declining sharply above 28 °C, signaling emerging productivity thresholds. NDVI exhibited consistent temperature sensitivity (Jaú, $R^2 = 0.32$; Tasmania, $R^2 = 0.43$) but weak precipitation relationships. Substantial tree cover loss occurred primarily in Tasmania and Yellowstone, coinciding with significant emission increases in Kahuzi-Biega, Crater Mountain, Yellowstone, Wolong, and Jaú ($R^2 = 0.35$–0.70; $p < 0.05$). Critically, despite rising emissions, most PAs remained net carbon sinks, except Gunung Leuser, which became a net carbon source despite minimal forest loss. Our findings indicate a critical decoupling between forest structure and carbon balance, underscoring the urgent need for adaptive strategies to safeguard ecological resilience in protected forests.

1. Introduction

Protected forest areas (PAs) represent critical nodes in the global ecological network, providing essential biogeophysical functions including biodiversity preservation, climate regulation, and carbon storage (Adams et al., 2023). As climate instability accelerates, their role has shifted from passive conservation sites to active agents of global mitigation and resilience. These ecosystems store vast quantities of aboveground biomass and continuously sequester atmospheric CO_2 through primary productivity (Zhao et al., 2022). By maintaining canopy cover and ecosystem function, forested PAs enhance both resilience and climate mitigation. Yet, their long-assumed role as persistent carbon sinks is increasingly challenged by global environmental pressures. Despite their recognized importance, the long-term carbon mitigation potential of PAs under climate change remains insufficiently quantified–limiting the development of targeted, evidence-based management strategies. This study addresses this gap by providing the first global assessment that integrates climate variability, vegetation dynamics, and carbon fluxes within forested PAs.

Originally designed to safeguard ecosystems from direct

* Corresponding author.
E-mail addresses: rezaul.karim@mail.utoronto.ca, kmrkarim2@gmail.com (M.R. Karim).

https://doi.org/10.1016/j.jenvman.2025.127916
Received 3 July 2025; Received in revised form 23 September 2025; Accepted 2 November 2025
Available online 5 November 2025

anthropogenic pressures, PAs aim to protect biodiversity from threats such as overexploitation, land-use change, pollution, and urban expansion–all of which continue to degrade habitats and intensify climate stressors (Mansourian et al., 2009). Despite major policy commitments–such as Aichi Target 11 to protect 17% of land and 10% of oceans by 2020–biodiversity loss persists, raising concerns about the effectiveness of existing conservation strategies. The Kunming-Montreal Global Biodiversity Framework (GBF) now aims to expand global PA coverage to 30% by 2030 (Arneth et al., 2023). However, expanding spatial coverage alone is unlikely to suffice without ensuring that these areas are ecologically functional and climate responsive. In particular, the capacity of PAs to deliver sustained carbon sequestration services remains poorly resolved.

Climate change has emerged as a dominant driver of ecological transformation in PAs, fundamentally altering temperature and precipitation regimes, which in turn influence forest productivity, species composition, disturbance frequency, and ecosystem functioning (Anderegg et al., 2020). Vegetation dynamics, as indicators of ecosystem function, can be assessed using Gross Primary Productivity (GPP) and satellite-derived proxies such as NDVI and EVI. These indices track photosynthetic activity, canopy greenness, and biomass accumulation (Wei et al., 2017; Gerard et al., 2020), and are essential for detecting ecological responses to climate stress.

However, growing evidence suggests that even protected ecosystems are not immune to large-scale ecological transitions. For example, up to 48% of Canada's terrestrial PAs may undergo biome-type shifts by the end of the century under elevated CO_2 and associated climatic changes (Lemieux and Scott, 2005). Such impacts vary by region–high-latitude ecosystems are especially sensitive to warming, while tropical and subtropical PAs face compounded pressures from both climate change and land-use transformation (Lee and Jetz, 2008). Notably, some protected forests buffer microclimatic extremes, especially in the tropics and boreal regions,reducing land surface temperatures by up to 20% relative to unprotected areas (Xu et al., 2022). These findings suggest that PAs may function as climate buffers, but it remains unclear whether this buffering capacity can persist under intensifying anomalies. Our framework uniquely combines structural indicators such as tree cover loss, with functional indicators, including NDVI, EVI, and GPP, to determine whether degradation in protected areas is primarily structural, functional, or both, an approach that has not previously been applied at the global scale.

To evaluate the resilience of PAs to these pressures, it is critical to monitor functional ecosystem responses over time. Tracking GPP, NDVI, and EVI across PAs enables the detection of changes in productivity and canopy condition under shifting climatic regimes. Datasets such as those from the Climate Research Unit (CRU) offer high-resolution, long-term records of temperature and precipitation (Harris et al., 2020), allowing for robust linkages between climatic anomalies and vegetation dynamics. However, inconsistencies in temporal coverage between climate and remote sensing datasets can introduce bias–for instance, when long-term climate data are compared with satellite metrics available only since 2001. To ensure analytical consistency and avoid misinterpretation, this study restricts all climate and vegetation analyses to a shared observational window from 2001 to 2023.

Beyond climate change, anthropogenic disturbance remains a pervasive threat to PA integrity. The degree to which PAs succeed in preventing deforestation and fragmentation is highly variable. In some regions, such as Spain, strict reserves have effectively limited land–cover expansion (Rodríguez-Rodríguez and Martínez-Vega, 2018). In contrast, only 26 of 48 national parks in East Africa maintained or gained forest cover (Pfeifer et al., 2012), underscoring disparities in enforcement and external pressure (Gizachew et al., 2018). Such threats often originate in surrounding landscapes but can quickly permeate protected boundaries, especially in poorly monitored areas.

The expansion of remote sensing technologies has revolutionized our ability to monitor these dynamics. The Hansen Global Forest Change dataset provides annual, high-resolution data on forest loss and regrowth globally (Hansen et al., 2013). It has proven effective in detecting even small-scale disturbances, such as slash-and-burn agriculture in Madagascar's Masoala National Park. However, its ability to detect subtle forms of degradation–such as selective logging–remains limited (Burivalova et al., 2015). When integrated with vegetation indices like NDVI and EVI, forest loss data offer a powerful means to assess whether structural and functional degradation occur concurrently or independently. Yet, care must be taken when using non-independent datasets, such as when forest loss data are also used to estimate carbon emissions.

Given the central role of forests in global carbon cycling, quantifying carbon fluxes within PAs is now a critical priority. Globally, PAs contain ~26% of all mapped terrestrial woody carbon stocks, amounting to ~61.43 Gt of aboveground carbon (Duncanson et al., 2023). While many PAs still function as net carbon sinks, this role is increasingly precarious. In regions of Brazil and Indonesia, severe forest degradation has already turned some PAs into net emitters (Collins and Mitchard, 2017). Moreover, carbon balance is not uniform even in intact forests, as it is shaped by factors such as climate variability, species composition, disturbance history, and edge effects (Liu et al., 2012). By directly linking climate anomalies, vegetation dynamics, and carbon flux models, this study provides an early-warning framework to detect when and why protected areas may shift from sinks to sources, thereby offering new insights for climate-smart conservation.

Understanding how and why these shifts occur is essential for targeted, climate-resilient conservation. Detecting tipping points–where forests transition from sinks to sources–requires the integration of long-term climate data with vegetation productivity indices. This is particularly important in PAs that maintain canopy structure but may be undergoing functional decline. By combining GPP, NDVI, EVI, and carbon flux models, researchers can gain a clearer understanding of the drivers of carbon balance change, supporting more adaptive PA management.

Given the diversity of biomes, legal protections, and management regimes across global PAs, conservation outcomes are far from uniform. The IUCN classifies PAs into categories ranging from strict nature reserves (Category I) to multiple-use landscapes (Category VI), each with distinct mandates (Supplementary Fig. 1). However, higher protection status does not guarantee reduced forest loss or emissions, as deforestation has been documented even within Category I reserves (Collins and Mitchard, 2017). Functional indicators–such as GPP, NDVI, and EVI–offer more nuanced and performance-based assessments of conservation effectiveness than protection status alone.

Despite the growing availability of remote sensing data, few studies have systematically evaluated the coupled effects of recent (post-2000) climate trends, vegetation dynamics, and carbon flux processes in globally distributed PAs. To bridge these critical knowledge gaps, this study investigates the extent to which climate trends influence forest productivity and carbon flux across global PAs by: (a) quantifying site-specific temperature and precipitation trends since 2001 and their influence on vegetation metrics (GPP, NDVI, EVI); (b) identifying the spatial patterns and drivers of tree cover loss within PAs; and (c) assessing whether PAs are retaining their net carbon sink function under observed climate and structural pressures. This integrated framework emphasizes data coherence, scale-appropriate analysis, and careful treatment of dataset dependencies–offering robust insights for climate-smart PA management.

2. Materials and METHODS

2.1. Study areas

This study examines eight protected forest areas (PAs) across multiple biogeographical realms, representing diverse climatic and ecological contexts (Fig. 1, Supplementary Table 1).

Yellowstone National Park (YNL) in the United States is located in

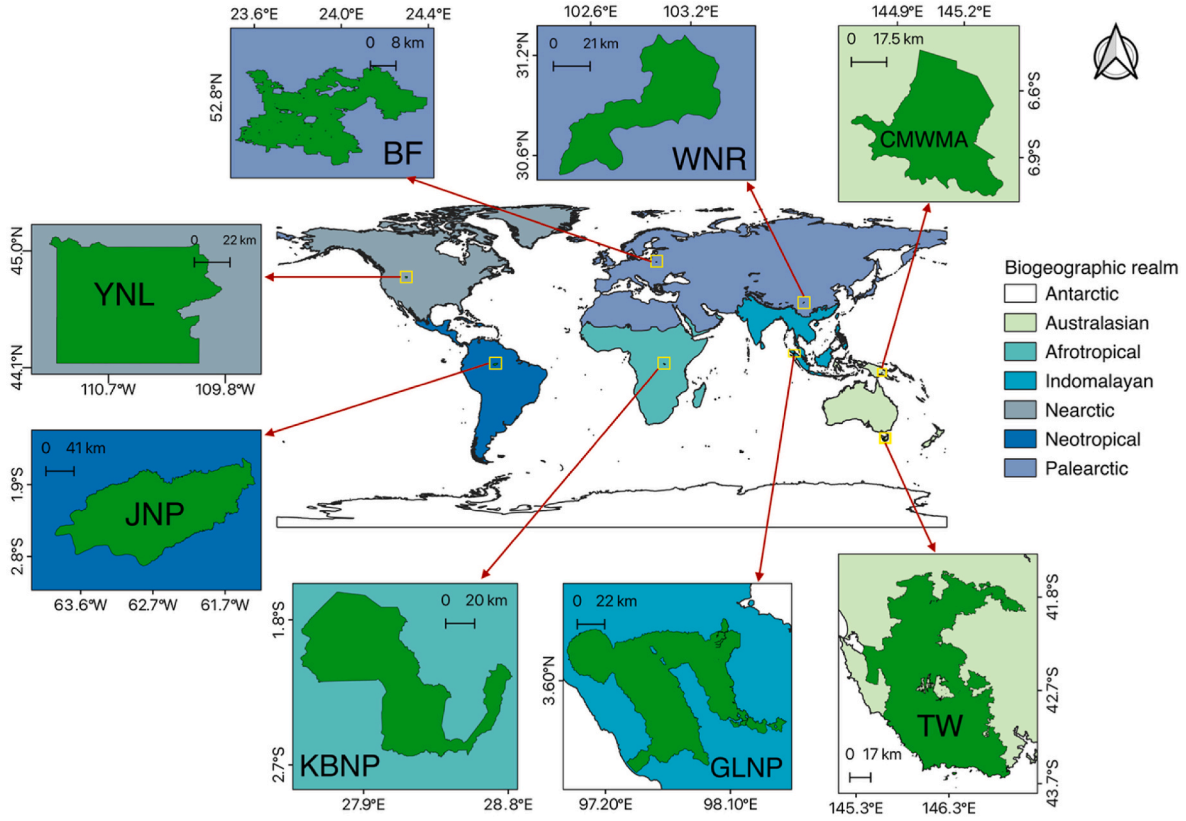

Fig. 1. Global distribution of the eight protected areas studied. The main panel shows the locations of the study areas across biogeographic realms: Nearctic, Neotropical, Palearctic, Afrotropical, Indomalayan, and Australasian. Insets detail each protected area: (1) Yellowstone National Park (YNL), (2) Jaú National Park (JNP), (3) Białowieża Forest (BF), (4) Kahuzi-Biega National Park (KBNP), (5) Wolong National Reserve (WNR), (6) Gunung Leuser National Park (GLNP), (7) Crater Mountain Wildlife Management Area (CMWMA), and (8) Tasmanian Wilderness (TW). Green denotes protected areas, with surrounding landscapes shaded by realm, illustrating their ecological diversity.

the Nearctic realm, dominated by *Pinus contorta* and *Pseudotsuga menziesii* (Buskirk, 2016). Białowieża Forest (BF), spanning Poland and Belarus, belongs to the Palearctic realm and features mixed temperate forests with *Quercus robur*, *Carpinus betulus*, and *Picea abies* (Jaroszewicz et al., 2019). Kahuzi-Biega National Park (KBNP) in the Democratic Republic of the Congo is part of the Afrotropical realm, characterized by montane and lowland rainforests with *Gilbertiodendron dewevrei* and *Entandrophragma excelsum* (Cirezi et al., 2025). Jaú National Park (JNP) in Brazil is located in the Neotropical realm, encompassing Amazonian rainforests dominated by *Eschweilera coriacea* and *Lecythis lurida* (Ferreira and Prance, 1998). Wolong National Reserve (WNR) in China and Gunung Leuser National Park (GLNP) in Sumatra, Indonesia, belong to the Indomalayan realm, with WNR featuring montane forests dominated by *Abies faxoniana* and *Betula albosinensis* (Liu et al., 2022), while GLNP contains tropical rainforests with *Dipterocarpus* spp. and *Shorea* spp (Susanti et al., 2021). Crater Mountain Wildlife Management Area (CMWMA) in Papua New Guinea is part of the Oceanian realm, comprising lowland to montane forests with *Castanopsis acuminatissima* and *Pandanus conoideus* (Dabek and Wells, 2021). Tasmanian Wilderness (TW) in Australia falls within the Australasian realm, featuring cool temperate rainforests dominated by *Nothofagus cunninghamii* and *Eucalyptus delegatensis* (Bowman et al., 2023). These sites collectively provide a globally relevant framework for assessing climate-driven vegetation dynamics and carbon flux variability in protected areas. To ensure spatial accuracy and global consistency, protected area boundaries were extracted from the World Database on Protected Areas (WDPA) (UNEP-WCMC and IUCN, 2025).

2.2. Climate data

We extracted monthly gridded climate data on temperature and precipitation from the Climatic Research Unit Time Series dataset (CRU TS v4.08; Harris et al., 2020), which provides global coverage at a spatial resolution of 0.5° × 0.5°. To maintain consistency with the temporal span of remotely sensed vegetation and carbon flux datasets, we limited our analysis to the period 2001–2023. For each protected area, monthly temperature values were averaged to derive annual mean temperature (MAT, °C), and monthly precipitation totals were summed to obtain total annual precipitation (AP, mm). Annual means and their standard errors were computed by grouping observations by site and year. Prior to trend estimation, we assessed whether ordinary least squares (OLS) regression was appropriate by testing for independence of residuals. Both the Durbin–Watson and Ljung–Box tests revealed strong positive autocorrelation in the annual series of temperature and precipitation (e.g., DW = 0.14 for MAT and DW = 0.37 for AP; Ljung–Box $p < 0.001$ in both cases), indicating that the OLS assumption of independent errors was violated. To accommodate this serial dependence, we employed generalized least squares with autoregressive errors of order 1 (GLSAR–AR1), implemented in Python's *'statsmodels'* package (v3.11.12).

The fitted model for each site and variable had the form of following equations Eq (1),

$$y_t = \beta_0 + \beta_1 t + \varepsilon_t \quad \text{(Eq 1)}$$

$$\varepsilon_t = \rho\varepsilon_{t-1} + \eta_t, \eta_t \sim \mathcal{N}(0, \sigma^2)$$

where y_t is MAT or AP in year t, β_1 is the annual trend (°C yr^{-1} or mm

yr^{-1}), and ρ is the first-order autoregressive coefficient. Parameters were estimated by iterative feasible GLS (10 iterations) until convergence. Residual independence in the initial OLS fit was evaluated using the Durbin–Watson statistic (Durbin and Watson, 1950); a substantial departure from the value 2 indicated positive or negative autocorrelation. For each model we report (i) the estimated slope β_1 (trend per year), (ii) its two-sided p-value, and (iii) the Durbin–Watson statistic to document the extent of residual autocorrelation. Pointwise 95% confidence intervals around fitted values were obtained from the GLSAR prediction intervals to illustrate uncertainty envelopes in figures. This approach yields trend estimates whose standard errors are correctly adjusted for temporal autocorrelation, thereby providing unbiased inference on the magnitude and direction of climate change within each protected area.

2.3. Vegetation data

To assess vegetation response to climate variability, we used Gross Primary Production (GPP; gC m^{-2} d^{-1}) data from the MODIS PML V2 Gridded Evapotranspiration 8-day composite, accessed via Google Earth Engine (GEE) (PML_V2 0.1.8). The dataset provides 500 m resolution GPP estimates from 2000 to 2023 and has been validated across 95 eddy covariance sites globally (Zhang et al., 2019). GPP was selected for its capacity to quantify photosynthetic carbon uptake at the ecosystem scale and its sensitivity to climatic variation. However, data are available from 2000, we defined the analysis period as 2001–2023 to ensure temporal consistency with the satellite and climate datasets.

We also analyzed the Normalized Difference Vegetation Index (NDVI) and Enhanced Vegetation Index (EVI), proxies for vegetation greenness and health essential for evaluating forest vitality and ecosystem responses (Kureel et al., 2022). NDVI and EVI were obtained from Landsat 5 (2001–2013) and Landsat 8 (2014–2023) via the Landsat Collection 2 Tier 1 Level 2 annual composite (30-m resolution; Crawford et al., 2023). NDVI was chosen for its robustness in quantifying vegetation cover and density, while EVI provides improved sensitivity in dense canopies and reduces atmospheric interference, making it well-suited for forest assessment. Annual mean NDVI and EVI were extracted in GEE to enable consistent site-level comparison. These indices were analyzed to detect vegetation trends and infer ecosystem stability and productivity shifts.

2.4. Forest cover change data

Forest loss was assessed using the Hansen Global Forest Change dataset (Hansen et al., 2013), offering 30-m resolution annual tree cover loss based on Landsat. This enables precise monitoring of forest degradation within protected areas. The dataset includes seven layers per 10° × 10° tile, each at 1 arc-second (~30 m) resolution. The *treecover2000* layer gives baseline canopy cover (percent of vegetation >5 m) for the year 2000. *Lossyear* records stand-replacement disturbances as values from 1 to 23 (2001–2023) or 0 (no loss).

We extracted *treecover2000* and *lossyear* for each site to assess spatial and temporal forest change. Analysis was conducted in GEE using asset ID: UMD/hansen/global_forest_change_2023_v1_11, allowing standardized assessment across protected areas.

2.5. Carbon dioxide (CO_2) flux data

We quantified CO_2 fluxes using the Global Forest Carbon Flux dataset (Harris et al., 2021), which provides annual spatial estimates of forest emissions and removals (2001–2023), based on satellite biomass data and ecological modeling in line with IPCC guidelines.

Net flux was calculated as the difference between emissions (from forest loss) and removals (from regrowth), with negative values indicating sinks and positive values sources. Removals account for CO_2 sequestration during regrowth, adjusted for forest type, ecozone, and age structure. Emissions include losses from all carbon pools. Disturbance years and forest loss activity were derived from the Hansen dataset (Hansen et al., 2013); thus, loss and flux data are not fully independent and were interpreted accordingly (see Discussion). Fluxes were calculated at 0.00025° × 0.00025° and aggregated to each protected area using GEE. To standardize comparisons, values were normalized by area and reported as $ktCO_2e/km^2$/year. Normalized fluxes were used in all analyses and supplementary assessments.

2.6. Statistical analyses

Temporal climate trends for 2001–2023 were quantified using linear regression applied to annual mean temperature (MAT) and total annual precipitation (AP) for each protected area. These analyses were implemented in R (v4.4.1) using the *'lm'* function, with slope coefficients, R^2 values, and p-values reported to assess the direction, strength, and significance of observed trends. All subsequent analyses were conducted also in R to ensure consistency and reproducibility. Relationships between Gross Primary Production (GPP) and climate variables were modeled using both linear and non-linear approaches, with model selection guided by Akaike Information Criterion (AIC) and Bayesian Information Criterion (BIC) to identify the best-fitting models (Table 1).

This dual modeling approach allows robust detection of both linear and non-linear responses of ecosystem productivity to climatic drivers. Forest cover loss patterns were analyzed using the raster package, enabling spatial quantification of annual tree cover loss for each protected area. To visualize and interpret carbon dioxide flux dynamics, we generated histograms of CO_2 fluxes and tree cover loss pixels (2001–2023 relative to the 2000 baseline) using *ggplot2*. This approach ensures reproducible, site-specific assessments of structural and functional ecosystem changes over time.

3. Results

3.1. Site-specific climate trends across protected areas (2001–2023)

Our analysis of annual mean temperature (MAT) and total annual precipitation (AP) from 2001 to 2023 revealed distinct site-specific trends across eight protected areas (PAs) (Fig. 2). Temperature trends varied among sites. Statistically significant increasing trends were observed at Białowieża Forest (BF) (slope = 0.063 °C yr^{-1}, $p = 0.011$), Crater Mountain Wildlife Management Area (CMWMA) (slope = 0.012 °C yr^{-1}, $p < 0.001$), and Tasmanian Wilderness (TW) (slope = 0.038 °C yr^{-1}, $p = 0.001$). Wolong National Reserve (WNR) also showed a significant but modest warming trend (slope = 0.016 °C yr^{-1}, $p = 0.026$). In contrast, trends at Yellowstone National Park (YNL) (slope = 0.032 °C yr^{-1}, $p = 0.323$), Kahuzi-Biega National Park (KBNP) (slope = 0.008 °C yr^{-1}, $p = 0.205$), Gunung Leuser National Park (GLNP) (slope = −0.001 °C yr^{-1}, $p = 0.907$), and Jaú National Park (JNP) (slope = −0.020 °C yr^{-1}, $p = 0.198$) were not statistically significant despite slight positive or negative trends in some cases.

Precipitation trends were highly variable among sites. Crater Mountain Wildlife Management Area (CMWMA) exhibited a significant decline in annual precipitation (slope = −1.49 mm yr^{-1}, $p = 0.004$), whereas Wolong National Reserve (WNR) showed a significant increase (slope = 0.60 mm yr^{-1}, $p = 0.002$). The remaining PAs–Yellowstone National Park (YNL) (slope = 0.19 mm yr^{-1}, $p = 0.180$), Jaú National Park (JNP) (slope = −0.93 mm yr^{-1}, $p = 0.677$), Białowieża Forest (BF) (slope = 0.11 mm yr^{-1}, $p = 0.685$), Kahuzi-Biega National Park (KBNP) (slope = 0.83 mm yr^{-1}, $p = 0.124$), Gunung Leuser National Park (GLNP) (slope = 0.67 mm yr^{-1}, $p = 0.133$), and Tasmanian Wilderness (TW) (slope = −0.17 mm yr^{-1}, $p = 0.725$)–did not show statistically significant changes, indicating largely stable precipitation patterns over the analysis period.

Collectively, these results suggest that warming trends are evident at multiple sites, with the strongest and most significant increases observed at BF, CMWMA, TW, and WNR. In contrast, statistically significant

Table 1
Model selection results for the relationship between Gross Primary Productivity (GPP) (gC m^{-2} d^{-1}) and climate variables (temperature and precipitation) across protected areas. Values of Akaike Information Criterion (AIC), Bayesian Information Criterion (BIC), and Residual Standard Error (RSE) are provided for linear, gaussian, quadratic, and cubic model fits. The best fit model is indicated by the lowest AIC and BIC values for each protected area.

Variables	Protected areas	Model	AIC	BIC	RSE
Temperature and GPP	YNL	Cubic	−726,655	−726,608	0.702316
	JNP	Linear	−2940,556	−2940,532	0.460873
	BF	Quadratic	−418,210	−418,180	0.344065
	KBNP	Linear	−437,300	−437,270	0.657210
	WNR	Gaussian	−19591.5	−19559.3	0.971695
	GLNP	Quadratic	233,017.6	233,051.7	1.198342
	CMWMA	Gaussian	107,960.1	107,991.3	1.250312
	TW	Quadratic	−1381,346	−1381,309	0.650224
Precipitation and GPP	YNL	Linear	−437,023	−437,000	0.74933
	JNP	Linear	−2031,089	−2031,064	0.613104
	BF	Linear	−275,882	−275,863	0.334977
	KBNP	Linear	−351,165	−351,142	0.739706
	WNR	Linear	143,843.4	143,864.9	1.233227
	GLNP	Linear	311,516.9	311,539.7	1.27144
	CMWMA	Linear	171,022.5	171,043.3	1.420019
	TW	Linear	808,770.7	808,795.5	1.246059

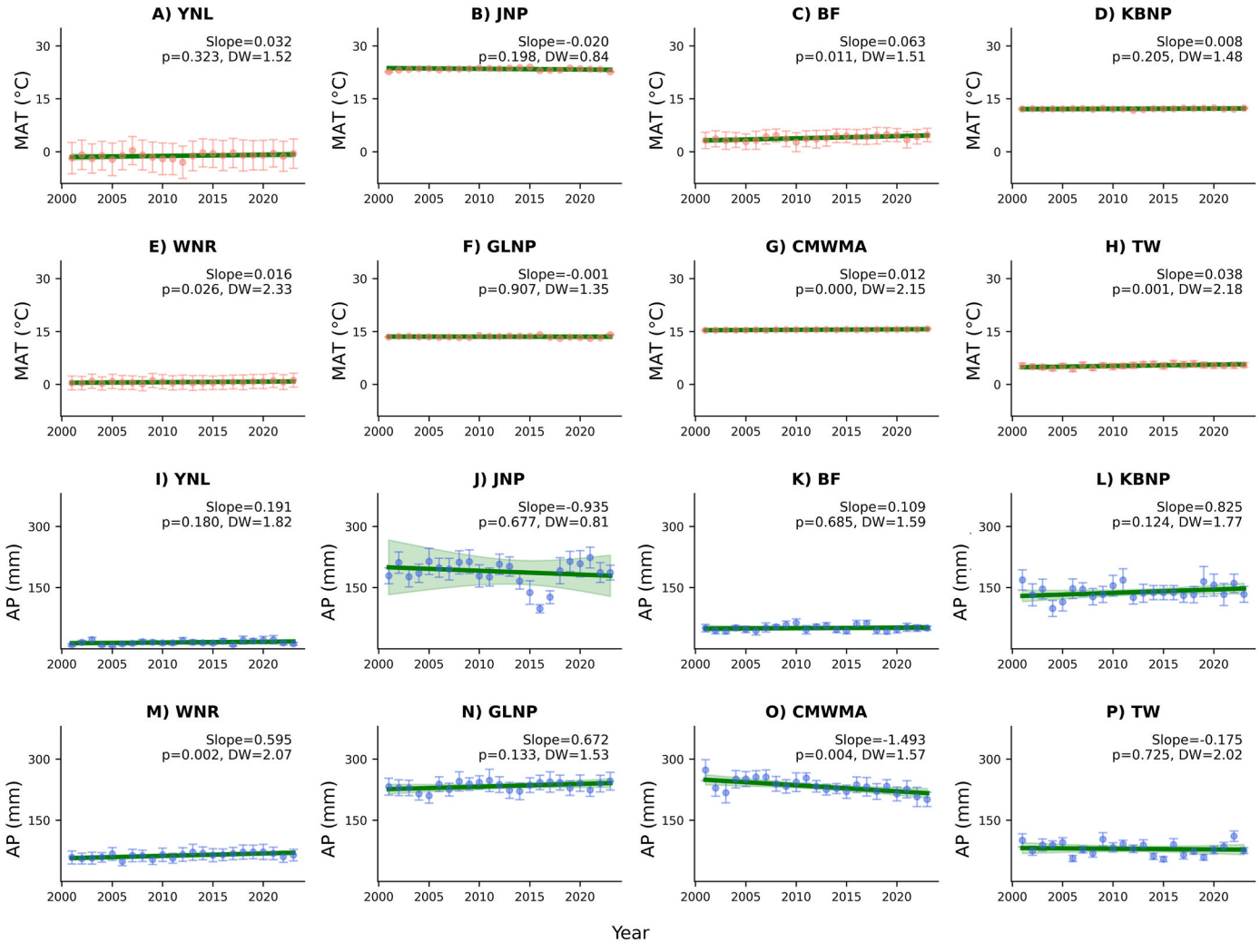

Fig. 2. Site-specific trends in annual mean temperature (MAT) and total annual precipitation (AP) from 2001 to 2023 across eight protected areas. Each panel shows site-level interannual variation with mean values (points) and standard error (error bars), overlaid with GLSAR regression trends (green lines) and 95 % confidence intervals (shaded areas). Temperature plots use salmon-colored points and error bars, while precipitation plots use royal blue. Slope, p-value, and Durbin-Watson statistic are annotated in the top-right of each panel. All data are derived from monthly aggregated values of the CRU TS 4.08 dataset.

changes in precipitation were limited to only two regions–one increasing (WNR) and one decreasing (CMWMA)–with most other sites exhibiting non-significant or negligible directional trends.

3.2. Climate-vegetation relationships across protected areas

The relationships between GPP and climate variables varied across the eight PAs (Fig. 3). The GPP exhibited a positive correlation with mean annual temperature in multiple sites. The strongest relationships were observed in BF ($p < 0.01$, $R^2 = 0.09$) and CMWMA ($p < 0.001$, $R^2 = 0.21$), where GPP increased with temperature. However, in some PAs such as TW ($p < 0.001$, $R^2 = 0.001$) and GLNP ($p < 0.01$, $R^2 = 0.05$), the relationships were relatively weak, indicating site-specific responses to temperature variation.

All fitted curves were constrained to observed climate ranges to avoid unsupported extrapolation. In YNL, for instance, GPP–temperature fits were restricted to the MAT range of −4 to 2.5 °C, aligning with empirical conditions. Similarly, modeled declines in GPP beyond 27–28 °C were not interpreted as site-level tipping points, but rather as theoretical upper bounds in warmer forests.

In contrast, the influence of annual precipitation on GPP was weak across most PAs, with marginal relationships observed in JNP ($p < 0.01$, $R^2 = 0.006$) and BF ($p < 0.001$, $R^2 = 0.07$). Notably, a negative correlation was detected at KBNP ($p < 0.001$, $R^2 = 0.38$), suggesting that increased precipitation may impose limitations on productivity in this ecosystem. The response in other sites, such as TW ($p < 0.01$, $R^2 = 0.006$), remained weak. These findings summarized that the temperature was a dominant predictor in temperate PAs, while precipitation effects were weaker, sometimes suppressive, indicating that moisture availability alone is not a sufficient predictor of productivity.

3.3. Vegetation indices and climate variability

The relationships between vegetation indices (NDVI and EVI) and climate variables were similarly heterogeneous across the eight PAs (Fig. 4). NDVI strongly increased with increasing temperature in several sites, including JNP ($p < 0.001$, $R^2 = 0.32$), BF ($p < 0.001$, $R^2 = 0.28$), KBNP ($p < 0.001$, $R^2 = 0.22$), GLNP ($p < 0.001$, $R^2 = 0.18$), and TW ($p < 0.001$, $R^2 = 0.43$). In contrast, EVI generally showed marginal or no correlation with mean temperature in WNR. However, at several sites–GLNP, KBNP, and TW–EVI exhibited comparable or stronger correlations than NDVI, with narrower confidence intervals.

This divergence highlights functional differences in how NDVI and EVI capture canopy responses in structurally complex forests. In montane sites with persistent cloud cover (e.g., WNR), EVI's insensitivity may reflect spectral noise or saturation.

The NDVI and EVI showed a strong positive correlation with precipitation in GLNP (NDVI: $p < 0.01$, $R^2 = 0.17$; EVI: $p < 0.05$, $R^2 = 0.18$), whereas the vegetation indices decreased with increasing precipitation in CMWMA (NDVI: $p < 0.01$, $R^2 = 0.19$; EVI: $p < 0.01$, $R^2 = 0.18$). These site-specific patterns reaffirm the non-universal nature of climate–vegetation coupling. Precipitation-driven greening was more evident

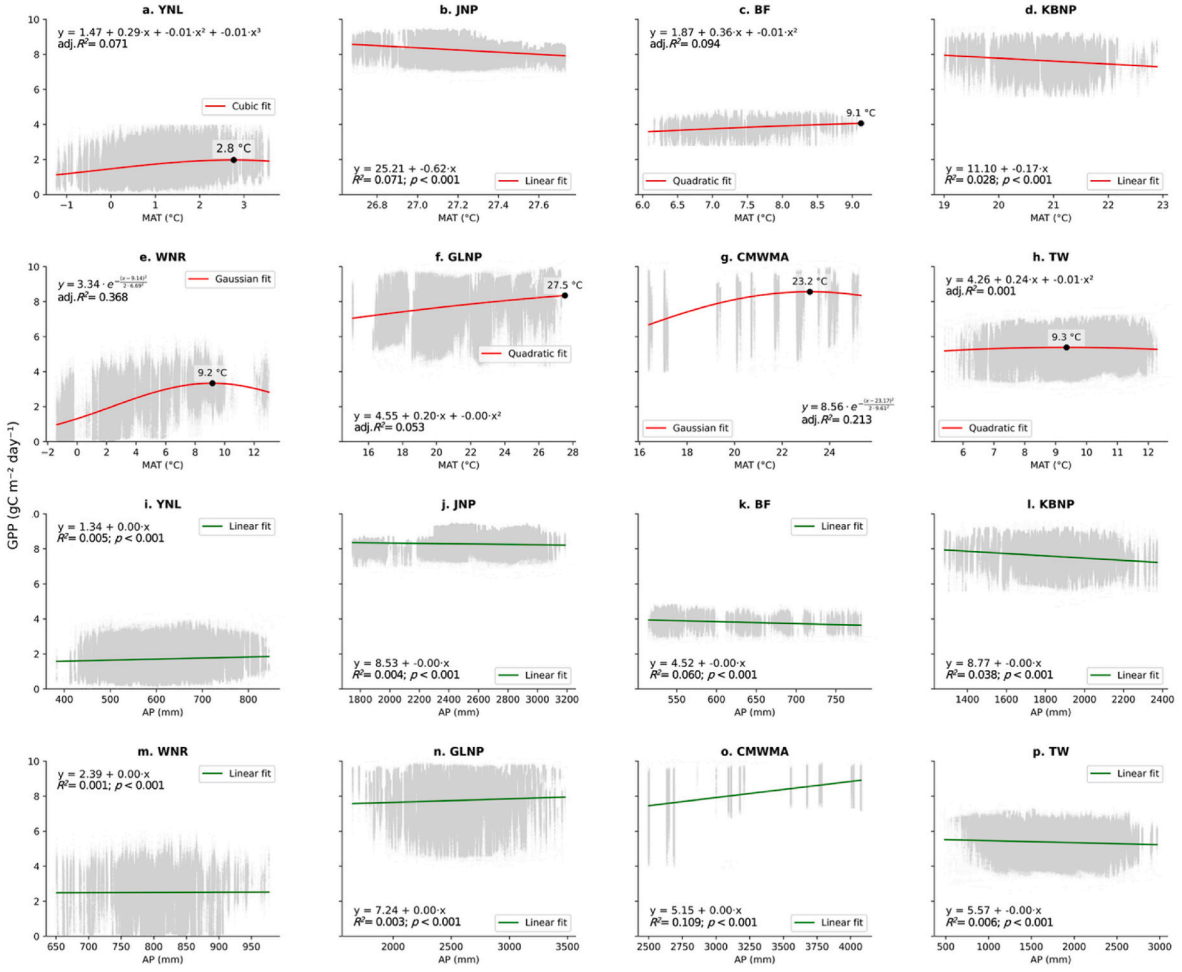

Fig. 3. Relationship between Gross Primary Production (GPP) and climatic variables across protected areas. The top row (a–h) shows the relationship between GPP and annual meana temperature (MAT), while the bottom row (i–p) presents the relationship between GPP and total annual precipitation (AP). Different curve-fitting approaches (linear, quadratic, cubic, and Gaussian) were applied as appropriate for each site.

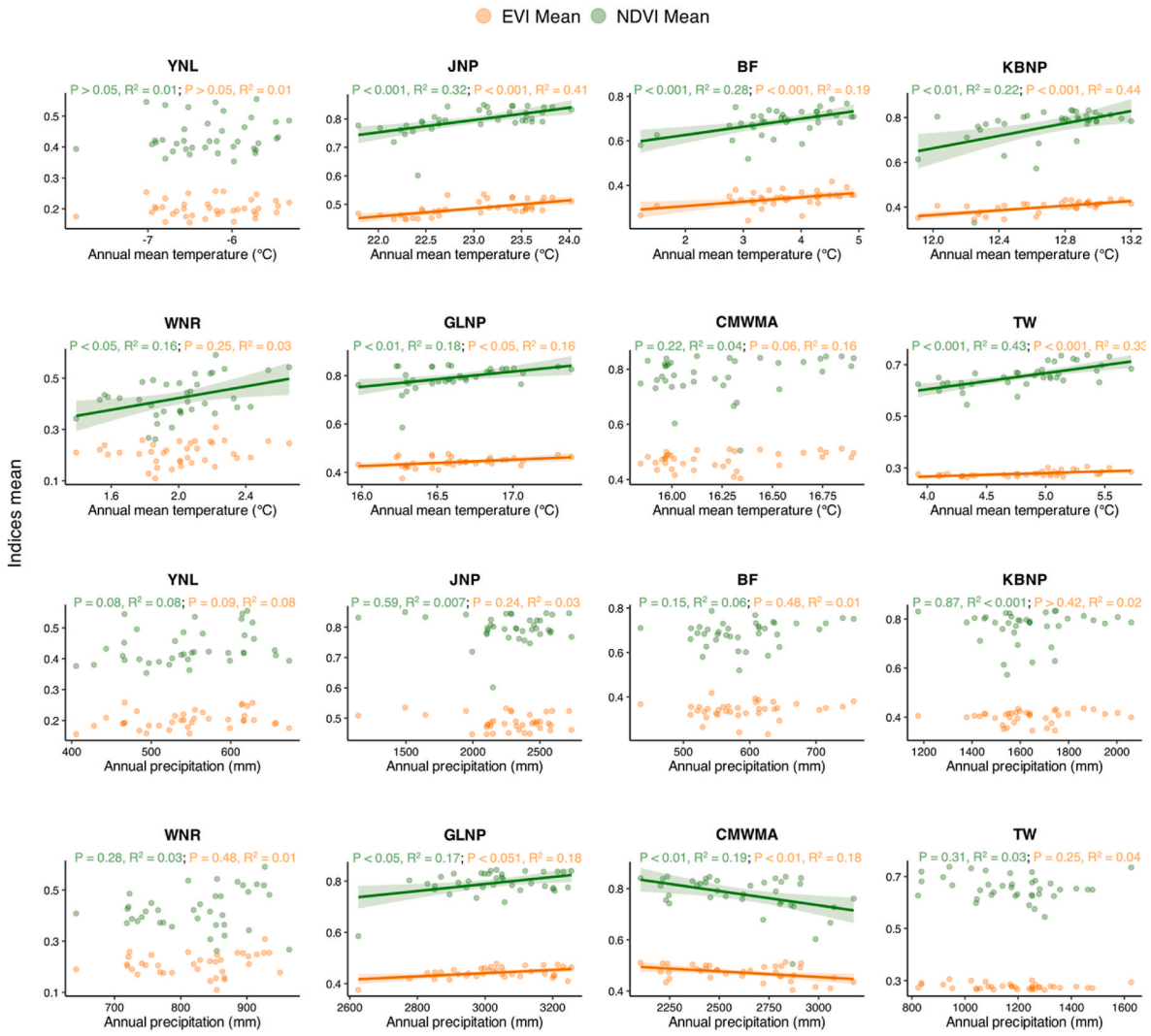

Fig. 4. Relationships between climate variables and vegetation indices across tropical and boreal protected areas. Scatter plots show the associations between annual mean temperature (°C) and total annual precipitation (mm) with mean NDVI (Normalized Difference Vegetation Index) and mean EVI (Enhanced Vegetation Index) across eight protected areas. Regression lines are displayed for significant relationships ($p < 0.05$), with shaded areas indicating 95% confidence intervals. Colors represent NDVI (green) and EVI (orange). Statistical significance and coefficient of determination (R^2) values are annotated for each relationship.

in equatorial rainforests (GLNP), whereas moisture stress may suppress vegetation indices in Oceania (CMWMA).

3.4. Spatial and temporal patterns of tree cover loss

All PAs experienced tree cover loss between 2001 and 2023, though rates varied considerably by site and year (Fig. 5). TW and YNL exhibited the highest loss rates, peaking at 1.3% in 2016. KBNP showed a gradual increase, reaching 0.52% in 2023. Conversely, WNR and JNP had minimal tree loss, with peaks of 0.1% and 0.12%, respectively. BF experienced episodic loss spikes (2.3% in 2016), while GLNP, CMWMA, and KBNP exhibited moderate but persistent degradation.

Regionally, temperate PAs lost significantly more canopy (0.30% ± 0.04) than tropical PAs (0.10 % ± 0.01; $p < 0.001$). Spatially, deforestation was often edge-focused or corridor-aligned (Fig. 6). In GLNP and KBNP, loss clustered along linear features, consistent with selective encroachment. In TW and YNL, core-area degradation suggests diffuse pressure, potentially from fire, pests, or windthrow.

The tree loss frequency also varied by initial canopy class. In YNL, loss was highest in areas with 80–85% initial cover, while BF peaked at 75–80%. GLNP exhibited a bimodal loss profile at 80% and 95% cover, indicating both mid-dense and dense canopies were vulnerable. These

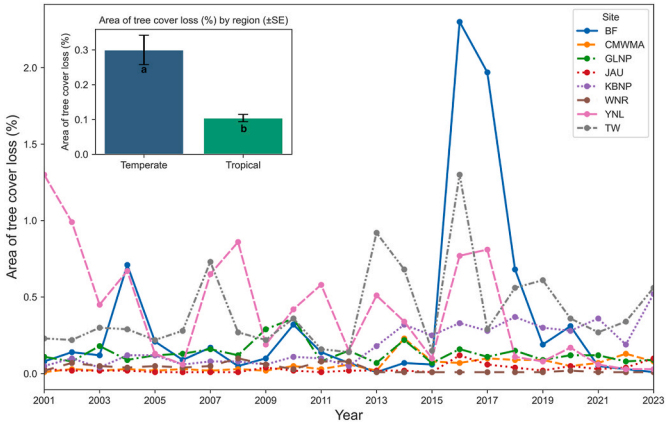

Fig. 5. Temporal variation in tree covers loss area (%) across eight protected areas (PAs) from 2001 to 2023. The main plot shows annual tree cover loss area (%) for each PAs, with different line styles and colors distinguishing the sites. The inset presents the mean tree cover loss area by region, with error bars indicating the standard error (±SE).

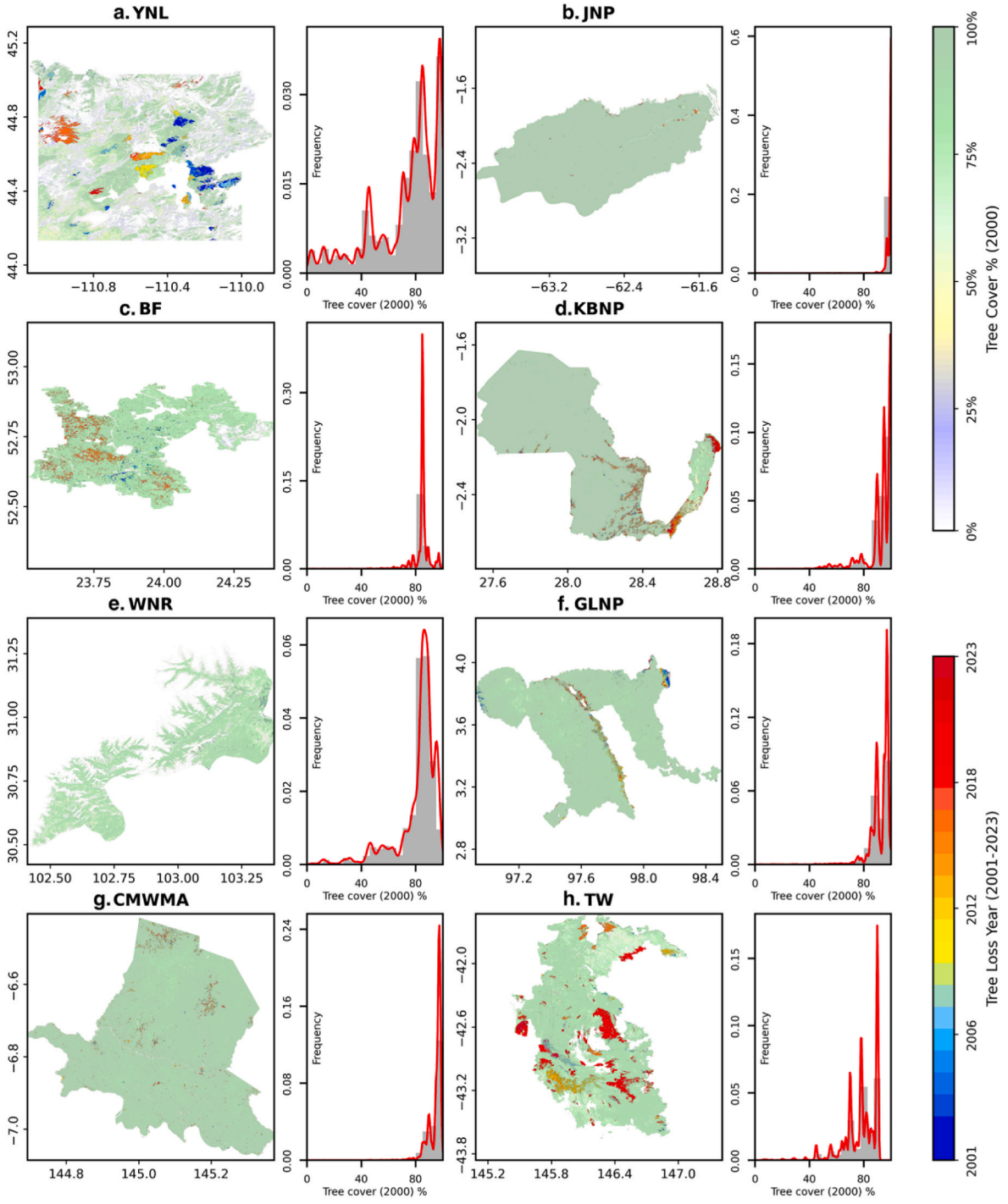

Fig. 6. Tree cover and loss across eight protected areas (PAs). Each PAs panel (left) displays tree cover in the year 2000 (green shades), with annual tree cover loss from 2001 to 2023 (colored pixels) based on Hansen Global Forest Change data. Warmer colors indicate more recent losses. The corresponding histogram (right) illustrates the distribution of tree cover (%) in 2000 and highlights the most vulnerable tree cover ranges that experienced loss during 2001–2023, with a red trendline representing the frequency distribution.

patterns indicate that forest structure, not just area, modulates sensitivity to disturbance.

3.5. Carbon emissions and net CO_2 flux trends across protected areas

Annual CO_2 emission trends from 2001 to 2023 revealed considerable site-level variation across the ten protected areas (PAs) (Fig. 7a–j). Statistically significant increases in annual emissions were observed in KBNP ($R^2 = 0.70$, $p < 0.001$), CMWMA ($R^2 = 0.59$), YNL ($R^2 = 0.50$), WNR ($R^2 = 0.37$), and JNP ($R^2 = 0.35$). Other sites–including TW, BF, and GLNP–showed weak or nonsignificant trends. Tropical PAs as a group exhibited a mild but significant rise ($R^2 = 0.05$, $p < 0.05$).

Despite rising emissions, most PAs retained net sink status over the study period. The strongest sinks were TW (−694.9 $tonCO_2e/km^2$/year), JNP (−204.8), and WNR (−132.4). CMWMA (−50.4) and KBNP (−13.7) also remained negative, though marginal. Notably, GLNP was the only protected area to function as a net carbon source (+197.9 $tonCO_2e/km^2$/year). This occurred despite a non-significant trend in emissions

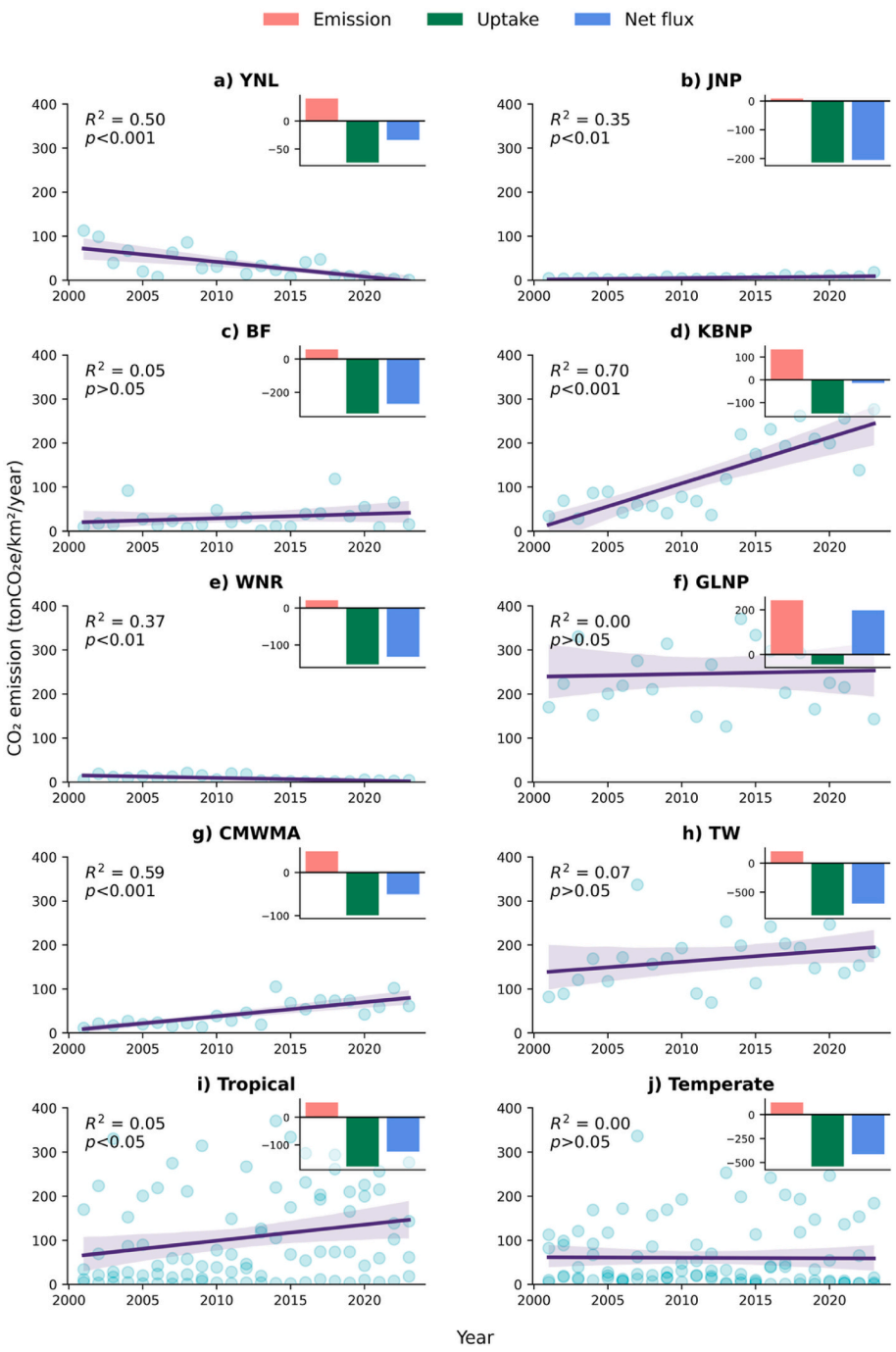

Fig. 7. Relationships between tree cover loss and CO_2 emissions across protected areas from 2001 to 2023. Panels (a) YNL, (b) JNP, (c) BF, (d) KBNP, (e) WNR, (f) GLNP, (g) CMWMA, and (h) TW illustrate site-level relationships between tree cover loss area (ha) and CO_2 emissions ($ktCO_2e$), with fitted linear regressions (red lines) and 95% confidence intervals (shaded areas). Panels (i) and (j) summarize these relationships for temperate and tropical regions, respectively. Insets show average annual greenhouse gas budgets over 2001–2023, with emission (red), uptake (green), and net flux (blue) components. Positive net flux indicates net emissions; negative values indicate carbon sinks.

from structural tree loss (Fig. 7f), indicating that factors other than canopy loss are the primary drivers of its net carbon balance.

These results challenge the assumption that structural loss is the dominant driver of emissions. The correlation between canopy loss and CO_2 emissions (R^2 = 0.75–0.99) must be interpreted cautiously, given shared data dependencies between the Hansen and Harris datasets. Functional degradation in structurally intact systems, such as GLNP, highlights the limits of using forest cover as a proxy for carbon stability.

4. Discussion

4.1. Long-term climate trends and implications for protected areas

Protected forest areas (PAs) are critical carbon reservoirs mediating biosphere–atmosphere exchanges and substantially contributing to terrestrial carbon sequestration (Duncanson et al., 2023). However, their functional stability faces increasing threats from climate-driven stressors and anthropogenic encroachments (Mansourian et al., 2009; Anderegg et al., 2020). This study identified significant heterogeneity in

climate trends, vegetation responses, and CO_2 fluxes across eight globally distributed PAs, highlighting the complexity of managing these ecosystems under climate change.

Significant long-term warming occurred in most PAs (e.g., CMWMA, BF, TW, WNR), aligning with broader regional warming signals (Higgins et al., 2023). The absence of warming in GLNP, JNP, YNL, and KBNP reflects local variability, likely driven by microclimatic buffering from topography, canopy structure, and elevation (Pepin et al., 2015; Johnson and Yeakley, 2019; Rita et al., 2021). These localized effects may help preserve climate-sensitive species. Nonetheless, persistent warming elsewhere risks vegetation stability, potentially triggering compositional shifts, wildfires, and pest outbreaks (Cunningham et al., 2024; Jones et al., 2024; Warlo and Kautz, 2024), threatening long-term carbon sequestration (Zhou et al., 2018).

Precipitation trends were more variable, with significant drying in CMWMA and increases in WNR, while others showed no clear change. However, precipitation variability alone did not consistently predict carbon flux patterns, as seen in contrasting responses in KBNP and YNL. This reflects complex ecohydrological interactions influenced by vegetation type, soil, rooting depth, and terrain (Anderson-Teixeira et al., 2011; Reyes et al., 2017; Desai et al., 2022). Thus, predicting vegetation responses requires integrating multiple climate variables and ecohydrological feedback, including soil moisture, vapor pressure deficit, and phenology.

These findings indicate substantial limitations in using climate trends alone to predict ecosystem productivity and carbon dynamics, highlighting the need for site-specific approaches to conservation planning. Future research should prioritize developing integrated climate-vegetation models incorporating local ecohydrological feedback mechanisms.

4.2. Vegetation dynamics and tree cover loss

Vegetation responses were highly site-specific, with temperature generally influencing NDVI and EVI more than precipitation. The divergence between NDVI and EVI at sites like WNR suggests each index captures different aspects of canopy dynamics, such as spectral sensitivity, phenology, or cloud cover effects (Karkauskaite et al., 2017; Ghebrezgabher et al., 2020). These spectral differences highlight the importance of using multiple vegetation indices for robust assessments under changing climates.

Tree cover loss further complicated vegetation–climate relationships. Substantial deforestation in TW and YNL appears linked to combined climatic and anthropogenic stressors (Clark et al., 2017; Mackey et al., 2017), while minimal loss in JNP and WNR may reflect effective protection or ecological resilience. However, localized losses along edges and corridors emphasize the influence of surrounding land-use, pointing to the need for buffer-zone management.

Global datasets often fail to capture subtle degradation (e.g., selective logging, understory loss), revealing gaps in current monitoring systems (Burivalova et al., 2015). Future improvements should include higher-resolution data and field validation to better detect fine-scale degradation.

4.3. Carbon dioxides sink potential and forest resilience in terms of vegetation cover

The spatiotemporal patterns of net CO_2 flux across PAs reflect complex interactions among climate variability, forest structure, and ecological resilience. Most PAs (TW, JNP, WNR, CMWMA) remained carbon sinks despite climatic and structural stress. For example, TW showed strong uptake despite canopy loss, suggesting mature forests and microclimatic buffering may mitigate disturbances (Prior et al., 2022). JNP and WNR, with minimal tree loss and stable climates, maintained sequestration, indicating intact canopies and sustained productivity (Kafy et al., 2023).

In contrast, the anomalous behavior of GLNP, which acted as a net carbon source despite stable forest cover, merits special attention. This decoupling of structural integrity from functional carbon sequestration points towards functional degradation, where the forest's metabolic processes are impaired. Potential underlying mechanisms include increased ecosystem respiration from soils and vegetation or decreased gross primary productivity due to climatic stressors (Zhang et al., 2025). Indeed, the broader region encompassing GLNP has been subject to documented periods of anomalous heat and drought over the past decade (Ramdani et al., 2024). Such conditions are known to reduce photosynthetic capacity and increase tree mortality, even without leading to immediate large-scale canopy loss. While a full attribution study is beyond the scope of this paper, our findings lead us to hypothesize that the net source status of GLNP is an early warning sign of climate-induced ecosystem stress. A formal factor analysis, correlating carbon flux with specific climatic variables (e.g., temperature, precipitation, soil moisture) as you suggested, represents a critical next step to test this hypothesis and pinpoint the exact causal mechanisms. Similarly, the shift at KBNP from a sink to near neutrality after 2014 further underscores the vulnerability of these ecosystems to the combined pressures of climate variability and incremental forest loss.

Overall, these patterns expose the inadequacy of canopy cover alone as a proxy for carbon stability. Supplementary Table 2 confirms this, highlighting that ecosystem fluxes depend on physiological processes (photosynthesis, respiration), phenological timing, and edaphic factors (e.g., soil moisture, nutrients), all dynamically shaped by climate. Future research should focus on physiological and phenological indicators, integrating field data, remote sensing, and ecosystem modeling to detect early degradation and ecological tipping points.

5. Implication on global protected areas conservation

This study stresses the need to restructure PA management frameworks to address the multi-dimensional challenges of climate change and forest degradation. Traditional approaches focusing on static boundaries and structural integrity (Wolf et al., 2021) are insufficient. The decoupling between structure and carbon dynamics at GLNP shows that functional indicators–like sequestration, productivity, and resilience—must be integrated into monitoring and planning.

Given the site-level heterogeneity in trends and fluxes, global conservation cannot rely on uniform strategies. Instead, region-specific interventions are needed. For instance, PAs like GLNP and JNP–facing warming but low structural loss–may benefit from assisted species migration, canopy thinning, or monitoring physiological stress. Conversely, drought-prone PAs (TW, CMWMA) may require reforestation with drought-tolerant species, soil moisture conservation, and ground-cover diversification (Groves et al., 2012).

Robust sequestration in JNP and WNR affirms the value of strict legal protection. Yet the carbon instability in KBNP despite moderate loss shows that protection alone is insufficient–functional monitoring must accompany structural assessments. Conservation frameworks should evolve to include real-time monitoring of vegetation indices, stress markers, and flux variability.

Important methodological limitations persist, especially the dependency between datasets used for forest loss and carbon flux estimation (Hansen et al., 2013; Harris et al., 2021). Future work should improve data independence via ground-based flux validation, high-resolution sensing, and phenological tracking. Standardized protocols using flux towers and carbon inventories could greatly enhance monitoring accuracy.

Successfully implementing adaptive, multi-objective conservation requires strong collaboration across policymakers, scientists, local communities, and interdisciplinary teams (Reside et al., 2018). Co-developed solutions–such as community-based restoration, adaptive zoning, and integrated buffer management–ensure ecological effectiveness and social sustainability. These approaches align conservation with

local socio-economic realities, enhancing resilience and long-term effectiveness.

In conclusion, the climate-driven changes observed in protected forests demand a shift toward adaptive, function-based conservation grounded in empirical monitoring and cross-disciplinary collaboration, ensuring continued delivery of climate mitigation and biodiversity services.

6. Conclusion

This study advances understanding of how climate-driven variability and forest dynamics influence vegetation productivity and carbon dioxide (CO_2) fluxes across globally distributed protected areas (PAs). By integrating climate data, vegetation indices (NDVI, EVI), gross primary productivity (GPP), and carbon flux analyses, we revealed distinct, site-specific ecological responses to recent climatic trends and disturbances. Our findings clearly demonstrate that forest carbon stability depends not only on structural attributes (e.g., canopy cover) but also critically on ecosystem functionality, physiological responses, and climatic thresholds. Most PAs maintained effective carbon sequestration despite experiencing climate stress and moderate canopy loss. However, notable exceptions, including Gunung Leuser National Park (GLNP) and Kahuzi-Biega National Park (KBNP), showed that carbon sink capacities could rapidly degrade under compound climatic and structural pressures. These outcomes highlight important limitations of current conservation strategies focused solely on structural preservation. Future research should address methodological uncertainties–especially those associated with remote sensing indices and the dependencies between datasets–through enhanced ground-based validation and refined modeling techniques. Moreover, incorporating physiological, phenological, and soil moisture variables into monitoring frameworks could substantially improve our ability to predict ecological thresholds and resilience under climate change. In summary, our findings advocate shifting towards adaptive conservation approaches that explicitly incorporate functional ecological indicators. This integrated perspective will help ensure that protected areas continue serving effectively as biodiversity reservoirs and global carbon sinks amidst accelerating environmental changes.

CRediT authorship contribution statement

Md Rezaul Karim: Writing – original draft, Visualization, Validation, Software, Methodology, Investigation, Formal analysis, Data curation, Conceptualization. **Elham Ashrafizadeh:** Writing – review & editing, Writing – original draft, Resources, Investigation. **Md Shamim Reza Saimun:** Writing – review & editing, Conceptualization. **Wenxi Liao:** Writing – review & editing, Validation. **Parvez Rana:** Writing – review & editing, Validation. **Mohammed AS. Arfin-Khan:** Writing – review & editing, Supervision.

Declaration of competing interest

The authors declare that they have no known competing financial interests or personal relationships that could have appeared to influence the work reported in this paper.

Acknowledgements

The authors declare that no specific funding was received for this research. We have no conflicts of interest to disclose. All analyses were conducted independently using publicly available datasets. We thank the data providers and open-access platforms that made this research possible.

Appendix A. Supplementary data

Supplementary data to this article can be found online at https://doi.org/10.1016/j.jenvman.2025.127916.

Data availability

Data will be made available on request.

References

Adams, V.M., Chauvenet, A.L.M., Stoudmann, N., Gurney, G.G., Brockington, D., Kuempel, C.D., 2023. Multiple-use protected areas are critical to equitable and effective conservation. One Earth 6, 1173–1189.

Anderegg, W.R.L., Trugman, A.T., Badgley, G., Anderson, C.M., Bartuska, A., Ciais, P., Cullenward, D., Field, C.B., Freeman, J., Goetz, S.J., 2020. Climate-driven risks to the climate mitigation potential of forests. Science 368, eaaz7005.

Anderson-Teixeira, K.J., DeLong, J.P., Fox, M.F., Brese, D.A., Litvak, M.E., 2011. Differential responses of production and respiration to temperature and moisture drive the carbon balance across a climatic gradient in New Mexico. Glob. Change Biol. 17, 410–424. https://doi.org/10.1111/j.1365-2486.2010.02269.x.

Arneth, A., Leadley, P., Claudet, J., Coll, M., Rondinini, C., Rounsevell, M.D.A., Shin, Y., Alexander, P., Fuchs, R., 2023. Making protected areas effective for biodiversity, climate and food. Glob. Change Biol. 29, 3883–3894.

Bowman, D.M.J.S., Ondei, S., Lucieer, A., Foyster, S., Prior, L.D., 2023. Forest-sedgeland boundaries are historically stable and resilient to wildfire at Blakes Opening in the Tasmanian Wilderness World Heritage Area, Australia. Landsc. Ecol. 38, 205–222. https://doi.org/10.1007/s10980-022-01558-x.

Burivalova, Z., Hassold, S., Fatroandrianjafinonjasolomiovazo, N.T., Bauert, M.R., Koh, L.P., 2015. Relevance of global Forest change data set to local conservation: case Study of Forest degradation in Masoala National Park, Madagascar. Biotropica 47, 267–274. https://doi.org/10.1111/btp.12194.

Buskirk, S.W., 2016. Wild Mammals of Wyoming and Yellowstone National Park. Univ of California Press, Oakland, CA.

Cirezi, N.C., Bastin, J.-F., Mugumaarhahama, Y., Useni, Y.S., Karume, K., Lumbuenamo, R.S., Bogaert, J., 2025. Analyzing drivers of tropical moist forest dynamics in the Kahuzi-Biega national park landscape, Eastern Democratic Republic of Congo from 1990 to 2022. Land 14. https://doi.org/10.3390/land14010049.

Clark, J.A., Loehman, R.A., Keane, R.E., 2017. Climate changes and wildfire alter vegetation of Yellowstone National Park, but forest cover persists. Ecosphere 8, e01636. https://doi.org/10.1002/ecs2.1636.

Collins, M.B., Mitchard, E.T.A., 2017. A small subset of protected areas are a highly significant source of carbon emissions. Sci. Rep. 7, 41902.

Crawford, C.J., Roy, D.P., Arab, S., Barnes, C., Vermote, E., Hulley, G., Gerace, A., Choate, M., Engebretson, C., Micijevic, E., Schmidt, G., Anderson, C., Anderson, M., Bouchard, M., Cook, B., Dittmeier, R., Howard, D., Jenkerson, C., Kim, M., Kleyians, T., Maiersperger, T., Mueller, C., Neigh, C., Owen, L., Page, B., Pahlevan, N., Rengarajan, R., Roger, J.-C., Sayler, K., Scaramuzza, P., Skakun, S., Yan, L., Zhang, H.K., Zhu, Z., Zahn, S., 2023. The 50-year Landsat collection 2 archive. Sci. Remote Sens. 8, 100103. https://doi.org/10.1016/j.srs.2023.100103.

Cunningham, C.X., Williamson, G.J., Bowman, D.M.J.S., 2024. Increasing frequency and intensity of the most extreme wildfires on Earth. Nat. Ecol. Evol. 8, 1420–1425. https://doi.org/10.1038/s41559-024-02452-2.

Dabek, L., Wells, Z., 2021. Chapter 10 - creating the first conservation area in Papua New Guinea to protect tree kangaroos. In: Dabek, L., Valentine, P., Blessington, J., Schwartz, K.R. (Eds.), Tree Kangaroos. Academic Press, pp. 135–151. https://doi.org/10.1016/B978-0-12-814675-0.00032-4.

Desai, A.R., Murphy, B.A., Wiesner, S., Thom, J., Butterworth, B.J., Koupaei-Abyazani, N., Muttaqin, A., Paleri, S., Talib, A., Turner, J., Mineau, J., Merrelli, A., Stoy, P., Davis, K., 2022. Drivers of decadal carbon fluxes across temperate ecosystems. J. Geophys. Res. Biogeosciences 127, e2022JG007014. https://doi.org/10.1029/2022JG007014.

Duncanson, L., Liang, M., Leitold, V., Armston, J., Krishna Moorthy, S.M., Dubayah, R., Costedoat, S., Enquist, B.J., Fatoyinbo, L., Goetz, S.J., 2023. The effectiveness of global protected areas for climate change mitigation. Nat. Commun. 14, 2908.

Durbin, J., Watson, G.S., 1950. Testing for serial correlation in least squares regression. I. Biometrika 37, 409–428. https://doi.org/10.1093/biomet/37.3-4.409.

Ferreira, L.V., Prance, G.T., 1998. Species richness and floristic composition in four hectares in the Jaú National Park in upland forests in Central Amazonia. Biodivers. Conserv. 7, 1349–1364. https://doi.org/10.1023/A:1008899900654.

Gerard, F.F., George, C.T., Hayman, G., Chavana-Bryant, C., Weedon, G.P., 2020. Leaf phenology amplitude derived from MODIS NDVI and EVI: maps of leaf phenology synchrony for Meso- and South America. Geosci. Data J 7, 13–26. https://doi.org/10.1002/gdj3.87.

Ghebrezgabher, M.G., Yang, T., Yang, X., Eyassu Sereke, T., 2020. Assessment of NDVI variations in responses to climate change in The Horn of Africa. Egypt. J. Remote Sens. Space Sci. 23, 249–261. https://doi.org/10.1016/j.ejrs.2020.08.003.

Gizachew, B., Solberg, S., Puliti, S., 2018. Forest carbon gain and loss in protected areas of Uganda: implications to carbon benefits of conservation. Land 7, 138.

Groves, C.R., Game, E.T., Anderson, M.G., Cross, M., Enquist, C., Ferdaña, Z., Girvetz, E., Gondor, A., Hall, K.R., Higgins, J., Marshall, R., Popper, K., Schill, S., Shafer, S.L., 2012. Incorporating climate change into systematic conservation planning. Biodivers. Conserv. 21, 1651–1671. https://doi.org/10.1007/s10531-012-0269-3.

Hansen, M., Potapov, P., Moore, R., Hancher, M., Turubanova, S.A., Tyukavina, A., Thau, D., Stehman, S.V., Goetz, S.J., Loveland, T.R., Kommareddy, A., Egorov, A., Chini, L., Justice, C.O., Townshend, J.R.G., 2013. High-Resolution global maps of

21st-Century Forest cover change. Science 342, 850–853. https://doi.org/10.1126/science.1244693.
Harris, I., Osborn, T.J., Jones, P., Lister, D., 2020. Version 4 of the CRU TS monthly high-resolution gridded multivariate climate dataset. Sci. Data 7, 109.
Harris, N.L., Gibbs, D.A., Baccini, A., Birdsey, R.A., de Bruin, S., Farina, M., Fatoyinbo, L., Hansen, M.C., Herold, M., Houghton, R.A., Potapov, P.V., Suarez, D.R., Roman-Cuesta, R.M., Saatchi, S.S., Slay, C.M., Turubanova, S.A., Tyukavina, A., 2021. Global maps of twenty-first century forest carbon fluxes. Nat. Clim. Change 11, 234–240. https://doi.org/10.1038/s41558-020-00976-6.
Higgins, S.I., Conradi, T., Muhoko, E., 2023. Shifts in vegetation activity of terrestrial ecosystems attributable to climate trends. Nat. Geosci. 16, 147–153. https://doi.org/10.1038/s41561-022-01114-x.
Jaroszewicz, B., Cholewińska, O., Gutowski, J.M., Samojlik, T., Zimny, M., Latałowa, M., 2019. Białowieża forest—a relic of the high naturalness of European forests. Forests 10. https://doi.org/10.3390/f10100849.
Johnson, A.C., Yeakley, J.A., 2019. Microsites and climate zones: seedling regeneration in the Alpine treeline ecotone worldwide. Forests 10. https://doi.org/10.3390/f10100864.
Jones, M.W., Veraverbeke, S., Andela, N., Doerr, S.H., Kolden, C., Mataveli, G., Pettinari, M.L., Le Quéré, C., Rosan, T.M., Van Der Werf, G.R., Van Wees, D., Abatzoglou, J.T., 2024. Global rise in forest fire emissions linked to climate change in the extratropics. Science 386, eadl5889. https://doi.org/10.1126/science.adl5889.
Kafy, A.-A., Saha, M., Fattah, MdA., Rahman, M.T., Duti, B.M., Rahaman, Z.A., Bakshi, A., Kalaivani, S., Nafiz Rahaman, S., Sattar, G.S., 2023. Integrating forest cover change and carbon storage dynamics: leveraging Google Earth Engine and InVEST model to inform conservation in hilly regions. Ecol. Indic. 152, 110374. https://doi.org/10.1016/j.ecolind.2023.110374.
Karkauskaite, P., Tagesson, T., Fensholt, R., 2017. Evaluation of the Plant Phenology Index (PPI), NDVI and EVI for start-of-season trend analysis of the northern hemisphere boreal zone. Remote Sens. 9. https://doi.org/10.3390/rs9050485.
Kureel, N., Sarup, J., Matin, S., Goswami, S., Kureel, K., 2022. Modelling vegetation health and stress using hypersepctral remote sensing data. Model. Earth Syst. Environ. 8, 733–748. https://doi.org/10.1007/s40808-021-01113-8.
Lee, T.M., Jetz, W., 2008. Future battlegrounds for conservation under global change. Proc. R. Soc. B Biol. Sci. 275, 1261–1270.
Lemieux, C.J., Scott, D.J., 2005. Climate change, biodiversity conservation and protected area planning in Canada. Can. Geogr. Géographe Can. 49, 384–397.
Liu, S., Zhou, T., Wei, L., Shu, Y., 2012. The spatial distribution of forest carbon sinks and sources in China. Chin. Sci. Bull. 57, 1699–1707.
Liu, X., He, L., He, Z., Wei, Y., 2022. Estimation of broadleaf tree canopy height of Wolong nature reserve based on InSAR and machine learning methods. Forests 13. https://doi.org/10.3390/f13081282.
Mackey, B., Cadman, S., Rogers, N., Hugh, S., 2017. Assessing the risk to the conservation status of temperate rainforest from exposure to mining, commercial logging, and climate change: a Tasmanian case study. Biol. Conserv. 215, 19–29. https://doi.org/10.1016/j.biocon.2017.08.032.
Mansourian, S., Belokurov, A., Stephenson, P.J., 2009. The role of forest protected areas in adaptation to climate change. Unasylva 60, 63–69.
Pepin, N., Bradley, R.S., Diaz, H.F., Baraer, M., Caceres, E.B., Forsythe, N., Fowler, H., Greenwood, G., Hashmi, M.Z., Liu, X.D., Miller, J.R., Ning, L., Ohmura, A., Palazzi, E., Rangwala, I., Schöner, W., Severskiy, I., Shahgedanova, M., Wang, M.B., Williamson, S.N., Yang, D.Q., Mountain Research Initiative EDW Working Group, 2015. Elevation-dependent warming in mountain regions of the world. Nat. Clim. Change 5, 424–430. https://doi.org/10.1038/nclimate2563.
Pfeifer, M., Burgess, N.D., Swetnam, R.D., Platts, P.J., Willcock, S., Marchant, R., 2012. Protected areas: mixed success in conserving East Africa's evergreen forests. PLoS One 7, e39337.
Prior, L.D., Foyster, S.M., Furlaud, J.M., Williamson, G.J., Bowman, D.M.J.S., 2022. Using permanent forest plots to evaluate the resilience to fire of Tasmania's tall wet eucalypt forests. For. Ecol. Manag. 505, 119922. https://doi.org/10.1016/j.foreco.2021.119922.
Ramdani, F., Setiani, P., Sianturi, R., 2024. Towards understanding climate change impacts: monitoring the vegetation dynamics of terrestrial national parks in Indonesia. Sci. Rep. 14, 18257. https://doi.org/10.1038/s41598-024-69276-9.
Reside, A.E., Butt, N., Adams, V.M., 2018. Adapting systematic conservation planning for climate change. Biodivers. Conserv. 27, 1–29. https://doi.org/10.1007/s10531-017-1442-5.
Reyes, W.M., Epstein, H.E., Li, X., McGlynn, B.L., Riveros-Iregui, D.A., Emanuel, R.E., 2017. Complex terrain influences ecosystem carbon responses to temperature and precipitation. Glob. Biogeochem. Cycles 31, 1306–1317. https://doi.org/10.1002/2017GB005658.
Rita, A., Bonanomi, G., Allevato, E., Borghetti, M., Cesarano, G., Mogavero, V., Rossi, S., Saulino, L., Zotti, M., Saracino, A., 2021. Topography modulates near-ground microclimate in the Mediterranean Fagus sylvatica treeline. Sci. Rep. 11, 8122. https://doi.org/10.1038/s41598-021-87661-6.
Rodríguez-Rodríguez, D., Martínez-Vega, J., 2018. Protected area effectiveness against land development in Spain. J. Environ. Manage. 215, 345–357.
Susanti, R., Pratama, B., Rahmawati, K., Suzuki, E., 2021. Preliminary study on plant ecology in Tangkahan Area, Gunung Leuser National Park. IOP Conf. Ser. Earth Environ. Sci. 762, 012020. https://doi.org/10.1088/1755-1315/762/1/012020.
UNEP-WCMC, IUCN, 2025. Protected planet: the world database on protected areas (WDPA) [WWW Document]. URL. https://www.protectedplanet.net.
Warlo, H., Kautz, M., 2024. How do global forest pests respond to increasing temperatures? – a meta-analysis. Oikos 2024, e10842. https://doi.org/10.1111/oik.10842.
Wei, S., Yi, C., Fang, W., Hendrey, G., 2017. A global study of GPP focusing on light-use efficiency in a random forest regression model. Ecosphere 8, e01724. https://doi.org/10.1002/ecs2.1724.
Wolf, C., Levi, T., Ripple, W.J., Zárrate-Charry, D.A., Betts, M.G., 2021. A forest loss report card for the world's protected areas. Nat. Ecol. Evol. 5, 520–529. https://doi.org/10.1038/s41559-021-01389-0.
Xu, X., Huang, A., Belle, E., De Frenne, P., Jia, G., 2022. Protected areas provide thermal buffer against climate change. Sci. Adv. 8, eabo0119.
Zhang, Q., Song, J., Nzinga, M.R., 2025. Climate change and forestry carbon sink: a literature review and visualization perspective. Front. For. Glob. Change 8, 1487503. https://doi.org/10.3389/ffgc.2025.1487503.
Zhang, Y., Kong, D., Gan, R., Chiew, F.H.S., McVicar, T.R., Zhang, Q., Yang, Y., 2019. Coupled estimation of 500 m and 8-day resolution global evapotranspiration and gross primary production in 2002 – 2017. Remote Sens. Environ. 222, 165–182. https://doi.org/10.1016/j.rse.2018.12.031.
Zhao, L., Du, M., Du, W., Guo, J., Liao, Z., Kang, X., Liu, Q., 2022. Evaluation of the carbon sink capacity of the proposed Kunlun Mountain National Park. Int. J. Environ. Res. Public. Health 19, 9887.
Zhou, R., Li, W., Zhang, Y., Peng, M., Wang, C., Sha, L., Liu, Y., Song, Q., Fei, X., Jin, Y., Gao, J., Lin, Y., Grace, J., Wang, S., 2018. Responses of the carbon storage and sequestration potential of Forest vegetation to temperature increases in Yunnan Province, SW China. Forests 9, 227. https://doi.org/10.3390/f9050227.